The Land Surface Climatology of the NCAR Land Surface Model Coupled to the NCAR Community Climate Model*

GORDON B. BONAN

National Center for Atmospheric Research,+ Boulder, Colorado

(Manuscript received 13 March 1997, in final form 17 July 1997)

ABSTRACT

The National Center for Atmospheric Research (NCAR) Land Surface Model (LSM, version 1.0) provides a comprehensive treatment of land surface processes for the NCAR Community Climate Model version 3 (CCM3). It replaces the prescribed surface wetness, prescribed snow cover, surface albedo, and surface flux parameterizations used in the CCM2. A 15-yr simulation of the coupled atmosphere (CCM3) and land (LSM1.0) models using observed sea surface temperatures for the period December 1978–September 1993 is used to document the model's land surface climate. The model simulates many of the observed geographic and seasonal patterns of surface air temperature, precipitation, and soil water. In general, the transition seasons (spring, autumn) are better simulated than winter and summer. Annual precipitation and runoff are well simulated for some river basins and poorly simulated for others. In general, precipitation is better simulated than runoff. The inclusion of net land–atmosphere CO_2 exchange is an important component of the land model, allowing it to be used for studies of the global carbon cycle. The model simulates annual net primary production that is consistent with other estimates of annual production. The model also simulates a clearly defined growing season based on temperature and soil water.

1. Introduction

The National Center for Atmospheric Research Land Surface Model (LSM version 1.0) provides a comprehensive treatment of land surface processes for the Community Climate Model version 3 (CCM3). It replaces the prescribed surface wetness and prescribed snow cover used in the CCM2. Instead, the land model has interactive hydrology in which soil water depends on water input from precipitation, dew, and snowmelt, water loss from evapotranspiration, and varies depending on soil physical properties that determine how much water infiltrates into the soil, how much water the soil can hold, and how much water drains from the soil. It also replaces the land surface fluxes and prescribed albedos in the CCM2, using instead parameterizations that include hydrological and ecological processes. The purpose of this paper is to document the model's performance in the CCM3.

Bonan (1996a) provides an in-depth description of the model, and Bonan (1996b) describes the effects of coupling the model to a precursor of the CCM3 that also used the CCM2 surface flux parameterizations. Compared to the CCM2 surface parameterizations, the land model improves the surface temperature simulation except for east Siberia in the winter, where the model exacerbates an existing warm bias, and high latitudes of North America, Europe, and Asia in the summer, where the model introduces a cold bias. The model has little impact on the vertical profiles of temperature and zonal wind. Differences in surface temperature generally do not extend into the atmosphere. The model has a much larger impact on specific humidity in July, with many regions showing a drier atmosphere; this drying extends up to 500 mb. There is little effect on atmospheric moisture in January. Many of the effects of the land model on the simulated climate appear to originate with its interactive hydrology.

2. Model description

The land model is a one-dimensional model of energy, momentum, water, and CO_2 exchange between the atmosphere and land, accounting for ecological differences among vegetation types, hydraulic and thermal differences among soil types, and allowing for multiple surface types including lakes and wetlands within a grid cell. Vegetation effects are included by allowing for 12 plant types that differ in leaf and stem areas, root profile,

* An electronic supplement to this article may be found on the CD-ROM accompanying this issue or at http://www.ametsoc.org/AMS.

+ The National Center for Atmospheric Research is sponsored by the National Science Foundation.

Corresponding author address: Gordon B. Bonan, National Center for Atmospheric Research, P.O. Box 3000, Boulder, Colorado 80307-3000.
E-mail: bonan@ncar.ucar.edu

height, leaf dimension, optical properties, stomatal physiology, roughness length, displacement height, and biomass. These 12 plant types form 28 different vegetated surfaces, each comprising multiple plant types and bare ground so that, for example, a mixed broadleaf deciduous and needleleaf evergreen forest consists of patches of broadleaf deciduous trees, needleleaf evergreen trees, and bare ground. Lakes and wetlands, if present, form additional patches. Soil effects are included by allowing thermal properties (heat capacity, thermal conductivity) and hydraulic properties (porosity, saturated hydraulic conductivity, saturated matric potential, slope of retention curve) to vary depending on percent sand and percent clay. Soils also differ in color, which affects soil albedos. Consequently, each grid cell in the domain of interest is assigned a surface type (which determines the patch fractions for each plant type), the fraction of the grid cell covered by lakes, the fraction covered by wetlands, soil texture (percent sand, silt, and clay), and soil color. For the T42 implementation of the CCM3, this surface dataset has a resolution of approximately 2.8° lat × 2.8° long.

Major features of the model are the following: prescribed seasonally varying leaf and stem areas; absorption, reflection, and transmission of solar radiation accounting for the different optical properties of plants, soil, water, snow, and ice; absorption and emission of longwave radiation allowing for emissivities less than one; sensible and latent heat fluxes, partitioning latent heat into evaporation of intercepted water, soil evaporation (which depends on soil water), and transpiration (which depends on stomatal physiology); turbulent transfer above and within plant canopies; vegetation and ground temperatures that balance the surface energy budget (net radiation, sensible heat, latent heat, soil heat); stomatal physiology and photosynthetic CO_2 uptake (which depend on absorbed photosynthetically active radiation, temperature, atmospheric CO_2 concentration, soil water, atmospheric vapor pressure, and foliage nitrogen); CO_2 losses during growth respiration (which is proportional to photosynthetic uptake), maintenance respiration from foliage, stem, and root biomass (which depend on temperature and also, for foliage biomass, nitrogen content, and soil water), and microbial respiration (which depends on soil water and soil temperature); interception, throughfall, and stemflow; snow hydrology; infiltration and runoff; temperatures for a six-layer soil column using a heat diffusion equation that accounts for phase change; soil water for the same six-layer column using a one-dimensional conservation equation (a form of Richards equation) that accounts for infiltration input, gravitational drainage at the bottom of the column, evapotranspiration losses, and vertical flow based on head gradients; and temperatures for shallow and deep lakes accounting for eddy diffusion and convective mixing.

The land model provides to the atmospheric model, at every time step, surface albedos (direct beam and diffuse for visible and near-infrared wavebands), upward longwave radiation, sensible heat flux, latent heat flux, water vapor flux, and surface stresses. The land CO_2 fluxes are not currently used by the CCM3. The CCM3 provides to the land model, at every time step, incident solar radiation (direct beam and diffuse for visible and near-infrared wavebands), incident longwave radiation, convective and large-scale precipitation, and lowest model-level temperature, wind, specific humidity, pressure, and height.

Bonan (1996a) provides a thorough description of the model and Bonan (1996b) describes the effects of coupling the model to a version of the CCM. Bonan et al. (1997) give comparisons between simulated and observed surface fluxes for three boreal forest sites in Canada. The model has been used to study land–atmosphere CO_2 exchange (Bonan 1995a), the sensitivity of the simulated climate to inclusion of lakes and wetlands (Bonan 1995b) and subgrid-scale runoff processes (Bonan 1996c), the effects of vegetation and soil (Kutzbach et al. 1996) and lakes and wetlands (Coe and Bonan 1997) on the African monsoon in the middle Holocene, and the effects of land use on the climate of the United States (Bonan 1997).

3. Results

Results are based on a 15-yr simulation of the coupled atmosphere (CCM3) and land (LSM1.0) models (hereafter referred to as simply the CCM3 simulation) using observed sea surface temperatures (SST) for the period December 1978–September 1993. Only the 14-yr period 1979–92 was analyzed. Initial conditions for the land (temperatures, snow, soil water) were obtained from December of year 10 of a 10-yr simulation that used climatological SSTs.

a. Surface temperature and precipitation

The Legates and Willmott (1990a) temperature climatology is used for comparison with the 2-m surface air temperature simulated by the model. The model has five pronounced cold biases throughout the year. Much of Antarctica and Greenland are too cold (by more than 10°C) throughout the year (Figs. 1–4). However, there are few observations in these regions and the quality of the polar climate must be assessed through additional analyses. The Tibetan Plateau region is also more than 10°C colder than the observations throughout the year and receives much more precipitation than is observed. The excessive precipitation is associated with orographic locking of precipitation, which causes a cold surface in the CCM even without the land model (Bonan 1996b). With the land model's interactive hydrology, the high precipitation results in deep snow accumulation in winter and wet soils in summer, causing a high latent heat flux, low sensible heat flux, and surface cooling. A similar problem occurs in the Andes Mountains of

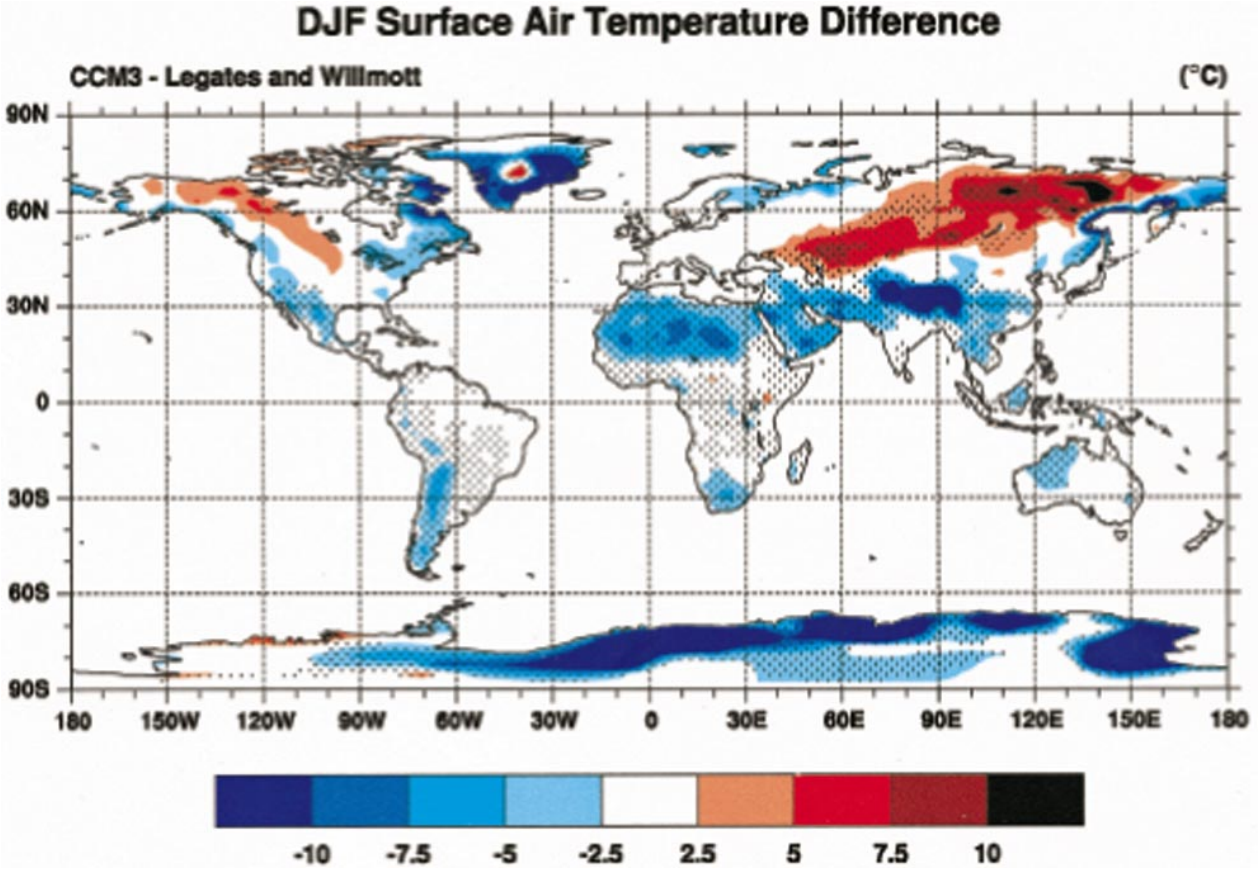

FIG. 1. Difference in surface air temperature averaged for the December–February season simulated by CCM3, coupled to LSM1.0, and the Legates and Willmott (1990a) climatology. Stippled areas show where the difference is more than twice the standard deviation based on the model's 14-yr climatology.

South America, which is several degrees too cold throughout the year. The Sahara Desert region of North Africa and the Arabian Peninsula are several degrees colder than the observations throughout the year. This bias is caused by high soil albedos, which were intentionally increased to match the high Earth Radiation Budget Experiment (ERBE) clear-sky albedos seen from space in this region. However, the high ERBE albedos may be caused by atmospheric aerosols and may not be indicative of surface albedos. If so, the land model overestimates surface albedo and the cold bias could be eliminated by lowering the model's soil albedos.

Tropical regions from 15°S to 15°N are well simulated throughout the year, with biases of less than 2.5°C. The desert regions of South Africa and Australia are well simulated in the transition seasons (spring, fall), but are too cold in winter and summer. Likewise, the model provides a better simulation of spring and fall in mid- to high latitudes of the Northern Hemisphere than it does in the winter and summer. In winter, temperatures are several degrees too warm in a band of North America extending from central Canada northwest to Alaska and in a broad band of Asia extending from the Caspian Sea northeast to far eastern Siberia. These warm biases are present in the CCM even without the land model, although the coupling with the land model accentuates the biases (Bonan 1996b). In summer, much of Alaska, northwest Canada, northern Europe, Russia, and western Asia are 2.5°–5°C too cold. The coupling of the land model to the CCM cools the surface in summer north of about 40°–50°N (Bonan 1996b), causing this cold bias.

Comparison of simulated and observed temperature and precipitation for each month of the year for specific regions gives further insight to the validity of the simulated surface climatology. In the Amazon Basin (Fig. 5), the observed temperatures fall within the model's interannual variability for most months. August and September are warmer than the observations, but only by about 2°C. The model also reasonably simulates the annual cycle of precipitation, resolving both the magnitude and duration of the dry season. The model is too dry prior to the start of the dry season and too wet after the dry season. The duration of the wet season is well simulated, although individual months differ greatly from the observations. Similar features occur in the Congo Basin and Indonesia, where the model reproduces the dry season better than the wet season.

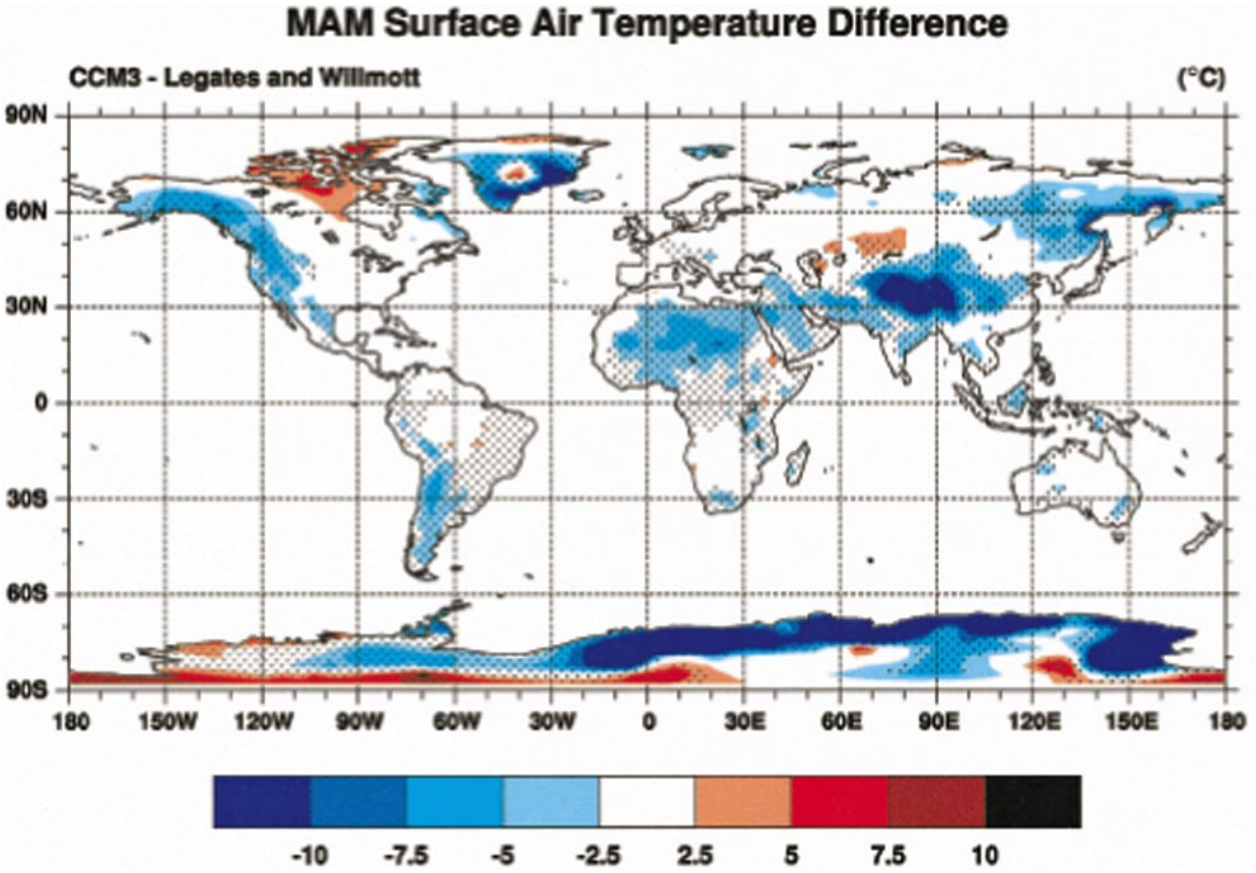

FIG. 2. As in Fig. 1 but for the March–May season.

In India (Fig. 6), the model is consistently several degrees too cold throughout the year. However, precipitation is very close to the observations in all months, and the model provides an especially good simulation of the magnitude, timing, and duration of the summer rainy season. The same is true for Central America, where the model is a few degrees too cold throughout the year, but precipitation is well simulated.

Arid regions are generally too cold, although precipitation is consistent with the observations. In the Sahara Desert (Fig. 7), the cold bias is due to the artificially high surface albedos needed to match satellite observations of clear sky albedo. However, this cold bias occurs in other desert and semiarid regions where albedos were not increased. For example, South Africa (Fig. 8) is too cold by about 3°C in June and July. Precipitation, however, is well simulated. Desert regions of South America and Australia have a similar cold bias but reasonable precipitation. The western United States (Fig. 9), which in this definition is mostly semiarid land, shows a cold bias throughout the year but reasonable precipitation.

The surface climatology of moist midlatitude regions (central and eastern United States, Europe) is fairly well simulated. For example, in central United States (Fig. 10) temperature is within a few degrees of the observations in all months. Precipitation is slightly underestimated in winter and autumn, but overall the model reasonably mimics the annual cycle, especially the summer precipitation.

In high-latitude regions, the model tends to be too warm in the winter and too cold in the summer. Precipitation is consistently overestimated. West Siberia (Fig. 11) illustrates this pattern, which is also found in Alaska, northwest Canada, northern Europe, and east Siberia.

b. Hydrology

The annual hydrologic cycle is examined in terms of precipitation and runoff for particular river basins (Table 1; Fig. 12). Globally, the model simulates 2.24 mm day^{-1} of precipitation over land, which agrees with the observations (Table 1). Forty percent of this precipitation (0.90 mm day^{-1}) runs off, which is slightly higher than Baumgartner and Reichel's (1975) estimate of 32%. Annual precipitation is particularly well simulated for certain river basins. For example, the model simulates 2.00 mm day^{-1} over the Mississippi River basin; the observations are 2.03 mm day^{-1}. The model is within

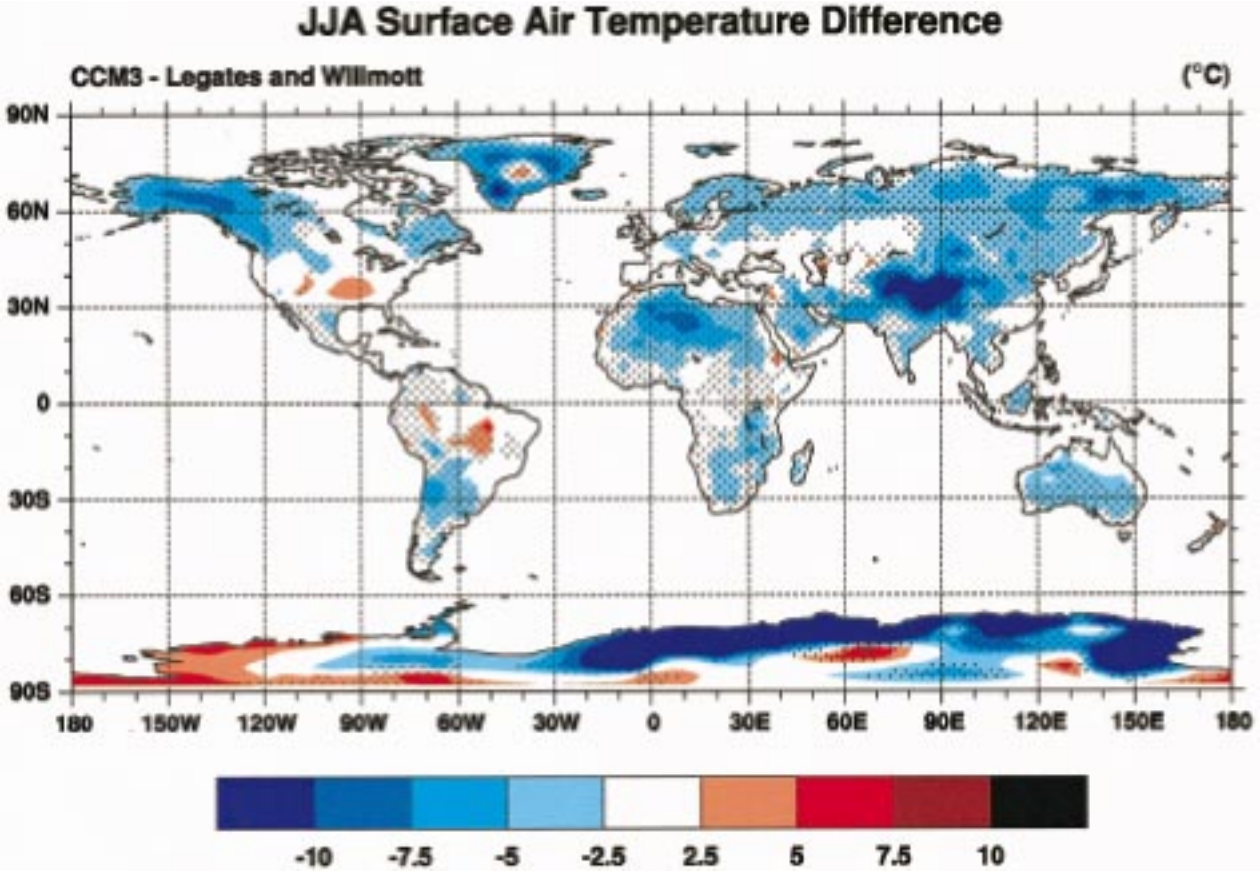

FIG. 3. As in Fig. 1 but for the June–August season.

8% of the observed precipitation for the Amazon River. Other basins are not well simulated. Precipitation is overestimated by more than 50% for the Congo, Mackenzie, and Yukon basins. When all 13 river basins are considered, however, the model accurately reproduces the annual precipitation. For the 13 basins, there is a statistically significant linear relationship between observed and simulated precipitation that accounts for 82% of the variance in the data and in which the intercept is not statistically different from zero and the slope is not statistically different from one—that is, there is a one-to-one correspondence between observed and simulated precipitation (Fig. 12).

Annual runoff is not as well simulated compared to observed river flow (Table 1). High-latitude basins in Siberia (Ob, Yenisey, Lena, Amur, but not Kolyma) are well simulated, but the Alaskan rivers (Mackenzie, Yukon) have too much runoff. In these two basins, there is excessive precipitation, which contributes to the excessive runoff. The Congo, when adjusted for the excessive precipitation, and Zambezi basins have too much runoff compared to observed river flow, which may reflect human removal of water. The Mississippi River is poorly simulated, with runoff equal to only one-third the observed river flow. This is 10% of the annual precipitation, whereas the observed river flow is almost one-third of the annual precipitation. When all 13 basins are considered, there is a statistically significant linear relationship between observed and simulated runoff, but it accounts for only 40% of the variance in the data (Fig. 12).

The coupling of the land model to the CCM cools the surface in summer north of about 40°–50°N (Bonan 1996b), causing a geographically extensive cold bias (Fig. 3). Bonan (1996c) demonstrated that for many regions the simulated surface air temperature is very sensitive to the model's infiltration parameterization, with high runoff resulting in dry soils, low latent heat flux, and a warm surface and low runoff having the opposite effects. One possible cause of this cold bias, then, is that the model allows too much water to infiltrate into the soil, creating wet summer soils and allowing a high latent heat flux that cools the surface. However, annual runoff is well simulated for four of the five river basins in Siberia. The two Alaskan rivers have too much runoff. So it appears that the model's partitioning of precipitation and snowmelt into runoff and infiltration is not the cause of the high-latitude cold bias.

Further insight to the cause of the cold bias can be obtained by comparing the hydrology in central United

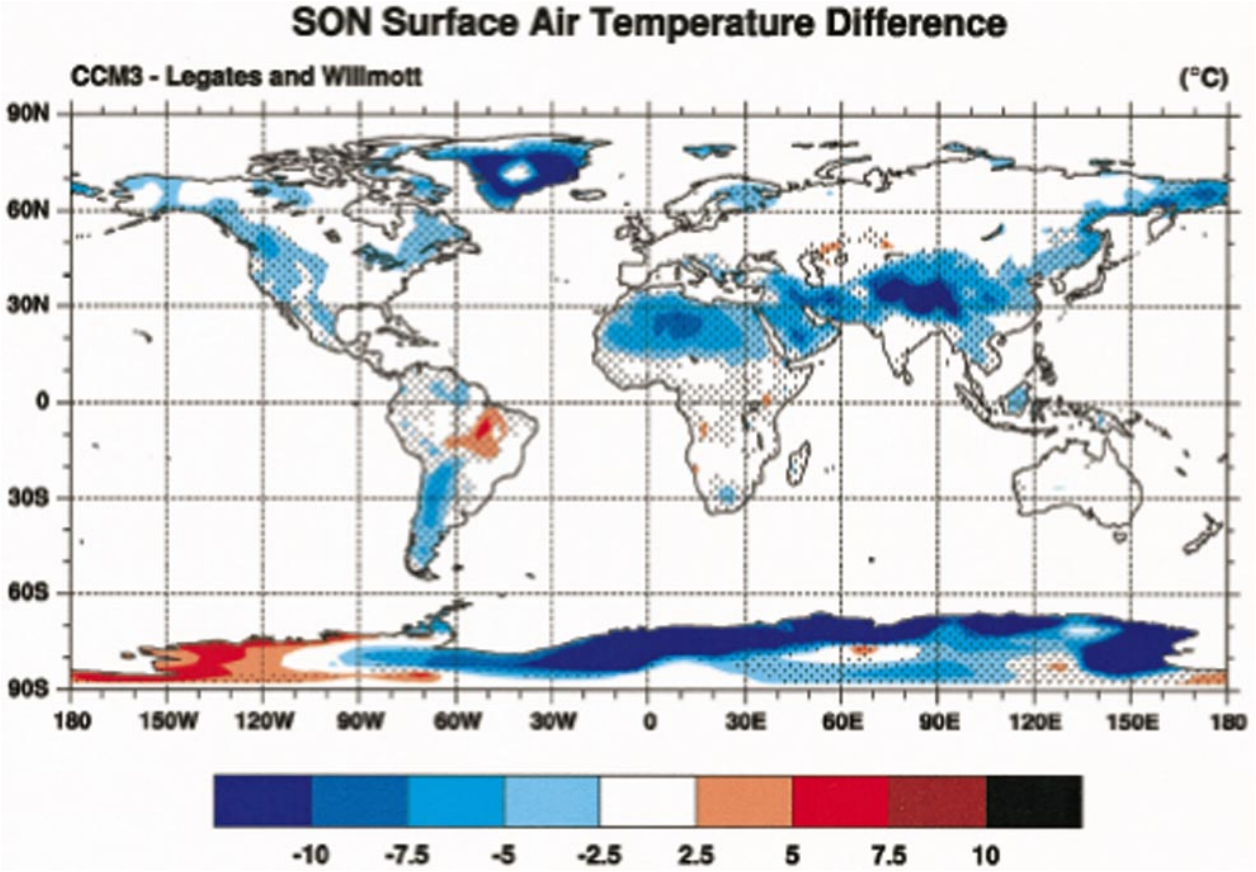

FIG. 4. As in Fig. 1 but for the September–November season.

States, eastern United States, and central Europe (three regions with small temperature biases) with regions where the temperature bias is large (Alaska and northwest Canada, northern Europe, western Siberia, and eastern Siberia) (Table 2). When examined in terms of a ''β factor'' that limits the latent heat flux, the soils are wetter during the summer in the cold regions than in the other regions. In addition, the cold regions have a higher latent heat flux, as a percent of net radiation, than the other regions. However, the wet soils are caused by lower annual evapotranspiration rather than excessive infiltration. As a percent of annual precipitation, the wet regions have slightly less infiltration (90%) than the other regions (92%). However, they have much less evapotranspiration (46% of annual precipitation) than the other regions (78%) and thus store more water in the soil, excluding subsurface drainage. One other possibly important difference between these two areas is that the cold regions have more precipitation than observed, whereas the other regions have less. This contributes to the wet soils, but also is likely to create more clouds, which reduces the solar radiation at the surface and cools the surface.

The model reproduces expected seasonal and geographic patterns of soil water, although there are few large-scale observations to provide guidance. In June, July, and August, tropical regions are very wet (Fig. 13). High-latitude regions of the Northern Hemisphere are also wet, especially throughout Canada and Russia, with a high abundance of lakes and wetlands. Polar deserts and regions of sandy soil (e.g., the Canadian Shield, northern Europe, and far east Siberia) have drier soils. The arid regions of the southwest United States, North Africa, Asia, South Africa, and Australia have some of the driest soils. Midlatitude regions of the United States and Europe have dry soils due to depletion of soil water during the growing season. These are the same general geographic patterns found with simple water budget models (Mintz and Walker 1993).

Seasonal analyses of the hydrologic cycle for specific regions show the model has the expected general features. In temperate and cold climates, soil water is depleted beginning in late spring and continuing through summer, with recharge in fall, winter, and early spring. Spring snowmelt is an important source of water to recharge the dry soils. In the Tropics, soils recharge during the rainy season.

For example, the desert soils of North Africa and the Arabian Peninsula are extremely dry (Fig. 14). Infiltration is relatively low except during the rainy season

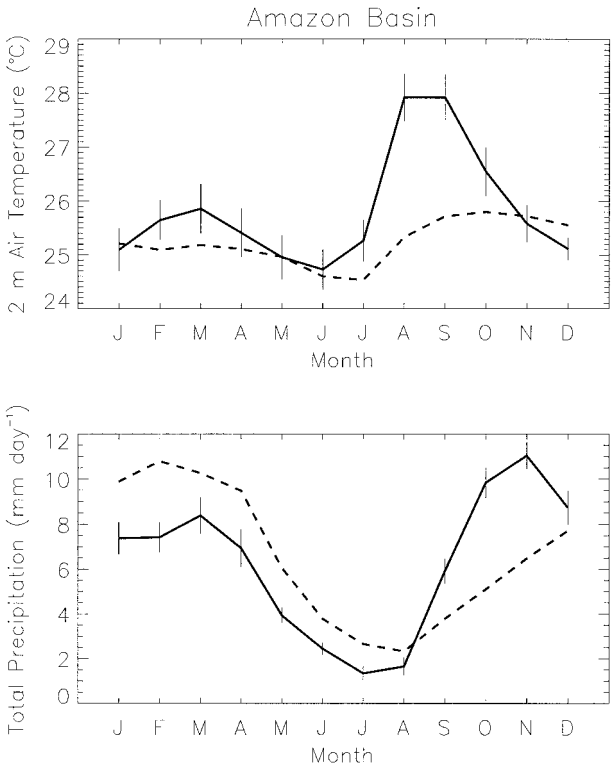

FIG. 5. Monthly simulated (solid) and observed (dashed) temperature and precipitation for the Amazon Basin region of South America. Observed temperature and precipitation are from the Legates and Willmott (1990a,b) climatology. Vertical bars indicate the model's 95% confidence interval for the mean based on the 14-yr climatology. The Amazon Basin is defined as all land points in a box from 10°S to the equator and 70°–50°W.

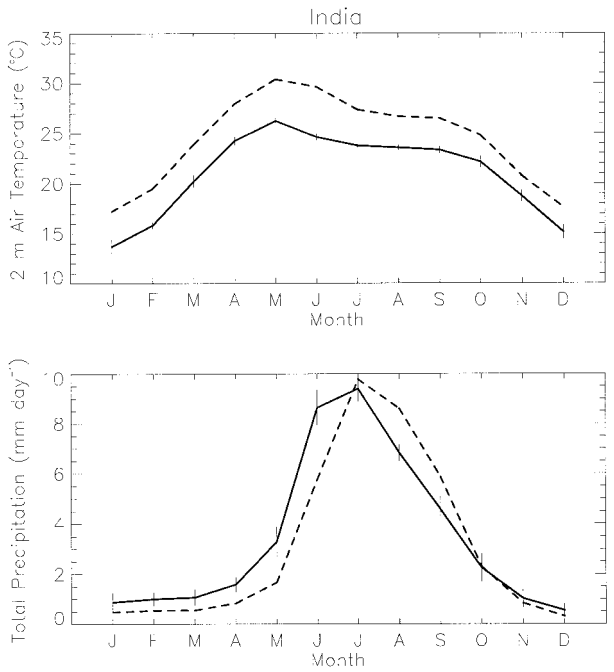

FIG. 6. As in Fig. 5 but for India (10°–30°N, 70°–90°E).

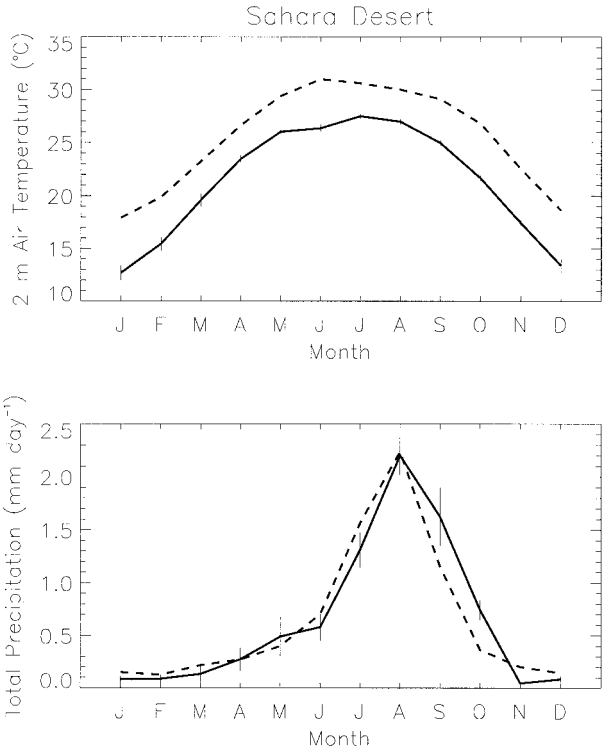

FIG. 7. As in Fig. 5 but for the Sahara Desert and Arabian Peninsula (10°–30°N, 20°W–50°E).

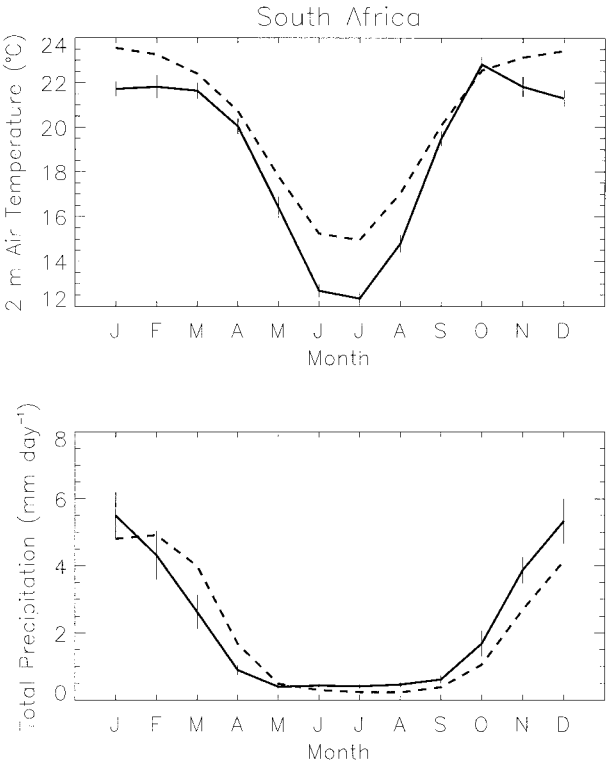

FIG. 8. As in Fig. 5 but for South Africa (35°–10°S, 10°–40°E).

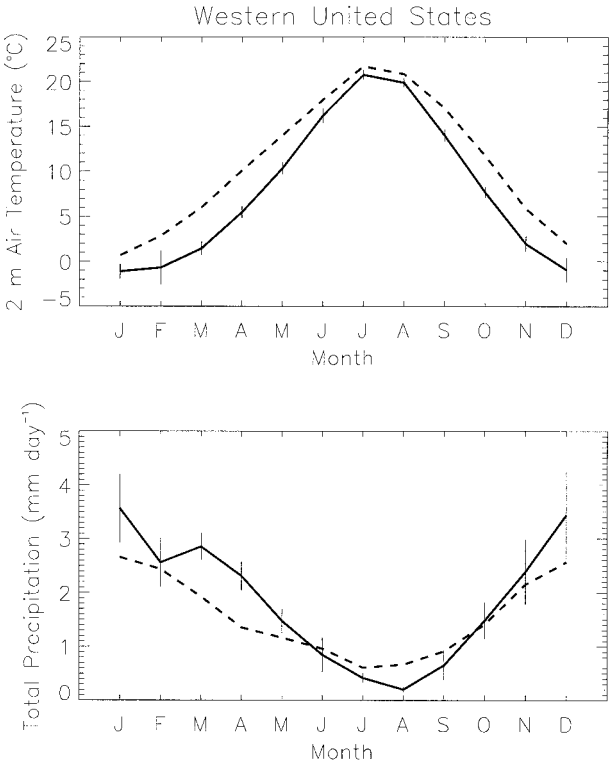

FIG. 9. As in Fig. 5 but for western United States (30°–50°N, 130°–110°W).

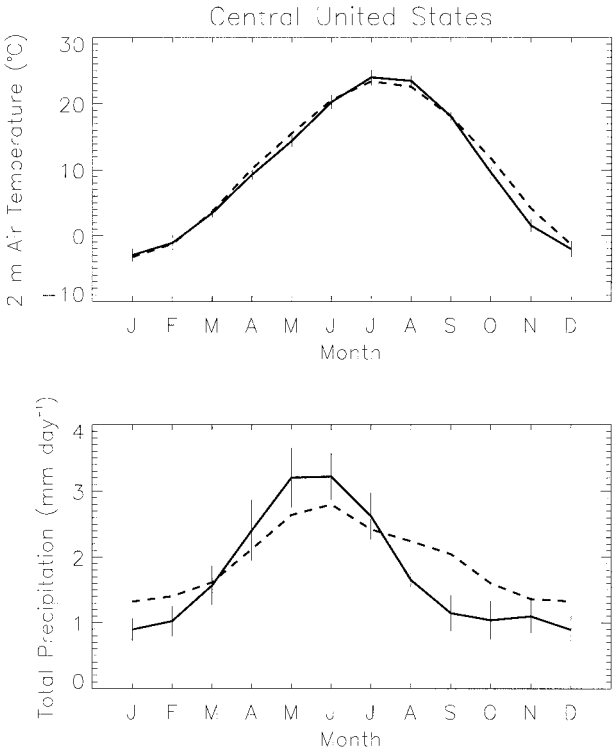

FIG. 10. As in Fig. 5 but for central United States (30°–50°N, 110°–90°W).

when the high rates of infiltration recharge the soil. Runoff is also small except during the rainy season. Maximum infiltration occurs in August, but maximum runoff occurs one month later, when the soils are wettest. In this dry region, sensible heat exceeds latent heat throughout the year.

In the Tropics (Fig. 15), soil water is high during the rainy season and depleted during the dry season. High rates of infiltration in the subsequent rainy season recharge the dry soils. During the rainy season about twice as much water enters the soil as is lost as runoff. Latent heat is about four times the sensible heat during the rainy season, but as the soil dries the latent heat flux decreases and sensible heating becomes dominant.

Central United States is typical of midlatitudes in the Northern Hemisphere (Fig. 16). Soil water decreases during the summer and recharges during fall, winter, and spring. Early spring snowmelt is an important source of water that recharges the soil. As the soil dries from June–September, the latent heat flux decreases and sensible heat flux increases.

East Siberia is typical of high-latitude regions (Fig. 17). Snow begins to accumulte in October, reaching maximum depth in March. Melt begins in April and is completed by June. Soil water recharges in late spring as the snow melts. The soil dries in the summer months when water input from precipitation is low and water loss from evapotranspiration is high.

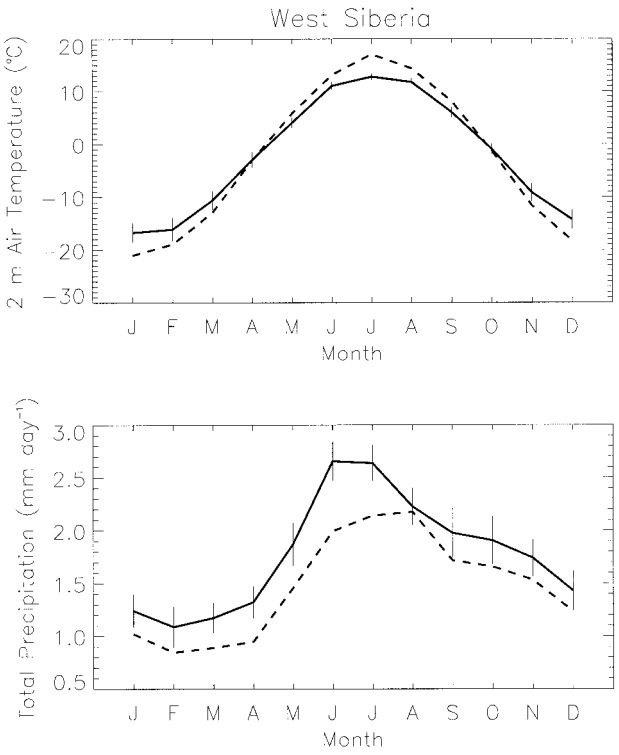

FIG. 11. As in Fig. 5 but for west Siberia (50°–70°N, 60°–90°E).

TABLE 1. Annual precipitation and runoff for selected drainage basins. Observed precipitation is from the Legates and Willmott (1990b) climatology. Observed basin runoff is river flow obtained from sources listed in Bonan (1996c). Global runoff is from Baumgartner and Reichel (1975).

Basin	Cells	Area (km²)	Precipitation (mm day⁻¹)		Runoff (mm day⁻¹)	
			Observed	CCM3	Observed	CCM3
Global land	2749	148 853 184	2.24	2.24	0.73	0.90
Amazon	80	5 510 292	6.19	5.71	2.69	1.94
Congo	52	3 060 214	4.55	6.73	1.19	2.84
Mississippi	50	2 411 034	2.03	2.00	0.63	0.21
Ob	61	2 304 330	1.41	1.74	0.46	0.50
Yenisey	71	2 235 598	1.23	1.65	0.69	0.72
Lena	73	2 152 146	1.08	1.33	0.65	0.68
Mackenzie	68	2 002 815	0.99	1.64	0.37	0.69
Zambezi	34	1 703 743	2.73	2.50	0.17	0.55
Amur	46	1 620 308	1.45	1.73	0.55	0.56
Orinoco	19	1 065 672	6.32	5.12	2.04	2.00
Ganges	20	1 028 659	3.38	2.72	1.30	0.72
Yukon	37	781 709	1.23	2.24	0.68	1.71
Kolyma	26	586 484	1.00	1.30	0.33	0.93

c. CO_2 fluxes

The land model simulates CO_2 uptake by terrestrial ecosystems during photosynthesis and CO_2 loss during plant and microbial respiration. In tropical regions, these fluxes have a seasonality associated with the wet and dry seasons. For example, in Amazonia (Fig. 18) CO_2 uptake is high during the wet season (October–May) and decreases during the dry season (June–September) as soil water is depleted. Plant respiration (leaf, stem, and root growth and maintenance respiration) shows a similar seasonality because the rate of leaf maintenance respiration is also tied to moisture availability. Microbial respiration increases during the dry season, perhaps because of the warmer soils, but is still a much smaller flux compared to photosynthesis and plant respiration. This region is a sink for CO_2 during the wet season and a source of CO_2 during the dry season.

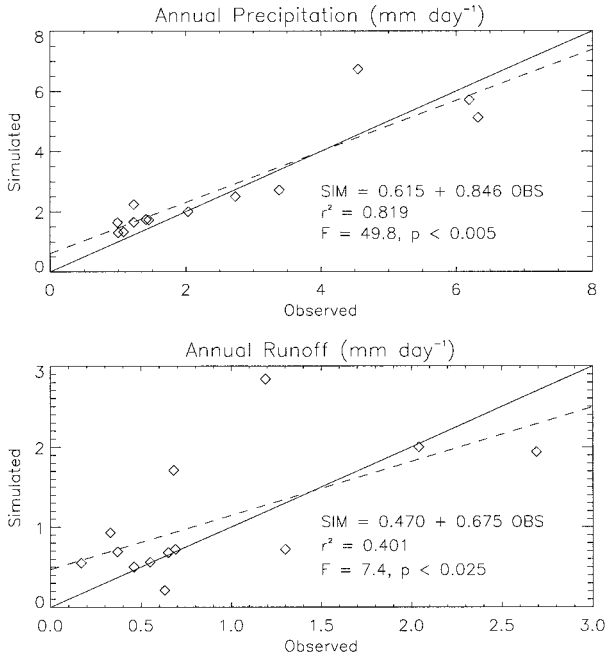

FIG. 12. Observed and simulated annual precipitation (top) and runoff (bottom) for the 13 river basins in Table 1. The solid lines show a one-to-one relationship. The dashed lines show the relationship obtained from a linear regression. Both regression relationships are statistically significant and have an intercept and slope that are not statistically different from zero and one, respectively. That is, there is a one-to-one relationship between observed and simulated data.

Temperate and high-latitude regions have a seasonality associated with temperature and water availability. In the central United States (Fig. 19), photosynthesis is low during winter, increases in spring, reaching peak rates in June and July, before it decreases as soil water is depleted. Plant and microbial respiration have strong temperature-dependent cycles, with low rates in cold months and high rates in warm months. Overall, this region is a source of CO_2 from August through April and a sink for CO_2 from May through July. Soil water does not limit photosynthesis in eastern Siberia. Instead, the annual cycles of photosynthesis and respiration respond to the strong temperature cycle (Fig. 20). The model simulates a clearly defined growing season in which there is a net uptake of CO_2 from May through September and CO_2 loss from October through April.

Bonan (1996b) gives a detailed analysis of these simulated fluxes and comparisons with observed net primary production and decomposition for LSM1.0 coupled to an earlier version of the CCM3. This atmospheric model differs from the final CCM3 in its convection scheme, using the CCM2 parameterization rather than the CCM3 parameterization. For the purposes of the following discussions, this atmospheric model is referred to as CCM3−. Table 3 shows annual net primary production averaged for different vegetation types for LSM1.0 coupled to CCM3− [Table 8 in Bonan (1996b)]. For comparison, Lieth's regression equations

TABLE 2. Summer [June–August (JJA)] and annual indicators of the hydrologic cycle for three midlatitude regions where the surface air temperature bias is small compared to the observations and four high-latitude regions where temperatures are too cold. Here β_e is an evaporation factor, ranging from one when the soil does not limit evaporation to zero when evaporation ceases. $\lambda E/R_n$ is the ratio of latent heat to net radiation. Precipitation, P, is given for both the observations (obs) and the model (sim). Here Q_{in} is the infiltration rate, E is evapotranspiration, and $Q_{in} - E$ is the storage of water in the soil, excluding subsurface drainage. It can be negative because some surface types (e.g., irrigated crops, lakes, wetlands) have an unlimited supply of water. Number in parentheses indicate hydrologic fluxes as a percent of the simulated precipitation.

	JJA seasonal averages			Annual fluxes (mm day^{-1})				
Region	Temperature bias (°C)	β_e	$\lambda E/R_n$	P (obs)	P (sim)	Q_{in}	E	$Q_{in} - E$
Central U.S.	0.4	0.486	0.521	1.91	1.73	1.56 (0.90)	1.58 (0.92)	−0.02 (0.01)
Eastern U.S.	−0.1	0.706	0.649	3.06	2.51	2.29 (0.91)	1.91 (0.76)	0.38 (0.15)
Central Europe	−1.4	0.434	0.487	2.30	2.21	2.06 (0.93)	1.56 (0.70)	0.50 (0.23)
Mean	−0.5	0.521	0.540	2.37	2.13	1.96 (0.92)	1.66 (0.78)	0.30 (0.14)
Alaska and northwest Canada	−4.4	0.924	0.612	1.50	2.10	192 (0.91)	0.80 (0.38)	1.12 (0.53)
Northern Europe	−3.2	0.960	0.716	1.88	2.13	1.91 (0.89)	0.93 (0.44)	0.98 (0.46)
Western Siberia	−3.0	0.843	0.672	1.47	1.77	1.59 (0.90)	1.00 (0.56)	0.59 (0.33)
Eastern Siberia	−4.4	0.897	0.588	1.15	1.49	1.32 (0.88)	0.79 (0.53)	0.53 (0.36)
Mean	−3.9	0.906	0.635	1.45	1.85	1.66 (0.90)	0.86 (0.46)	0.80 (0.43)

between net primary production and mean annual air temperature and annual precipitation are used to estimate productivity from observed temperature and precipitation [see Bonan (1995a) and (1996b) for more details]. The model gives results similar to Lieth's estimates for most vegetation types. Where the model differed appreciably (e.g., needleleaf evergreen forest, broadleaf deciduous forest, savanna, grassland, and tun-

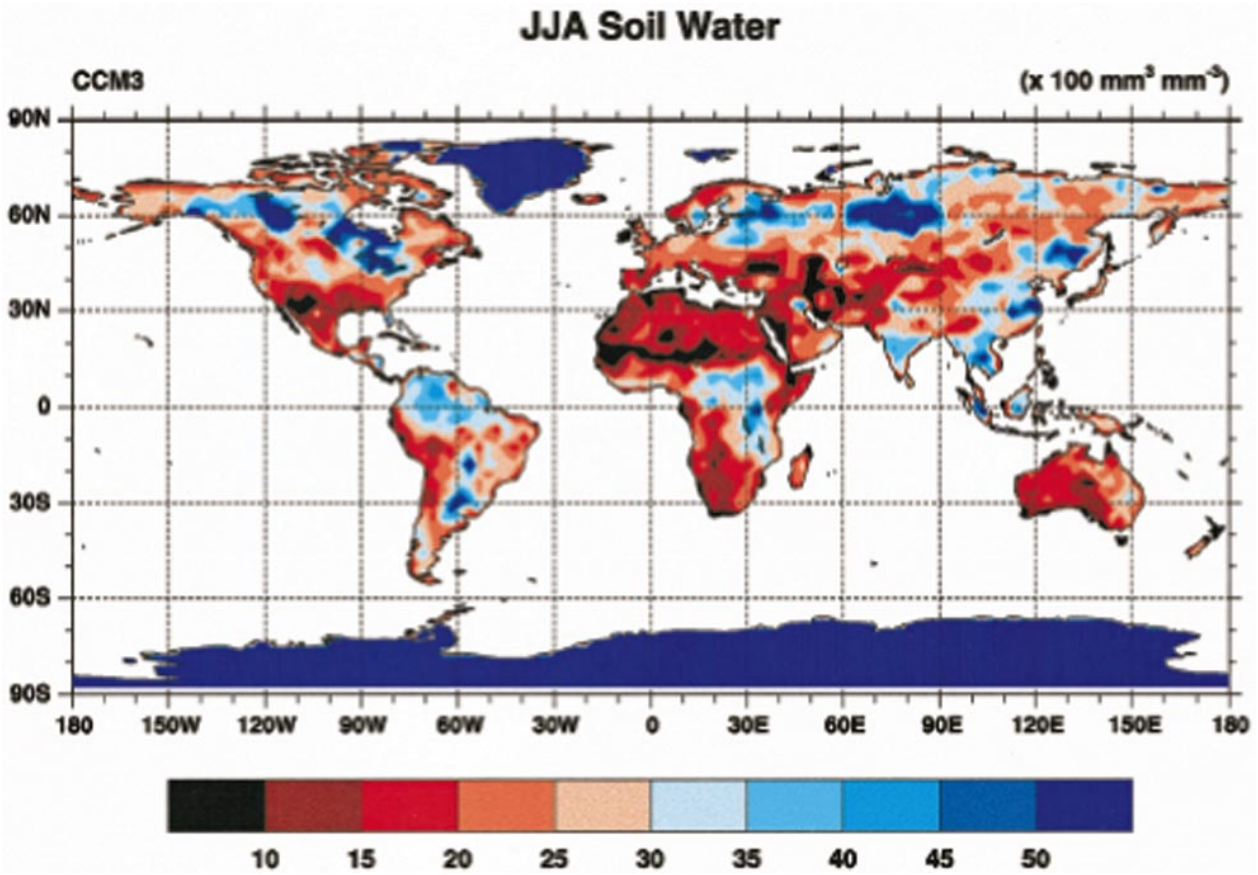

FIG. 13. Volumetric soil water (mm^3 water mm^{-3} soil) in the top 70 cm of soil averaged for June–August. Glaciers (Greenland, Antarctica) have water contents equal to 1.0.

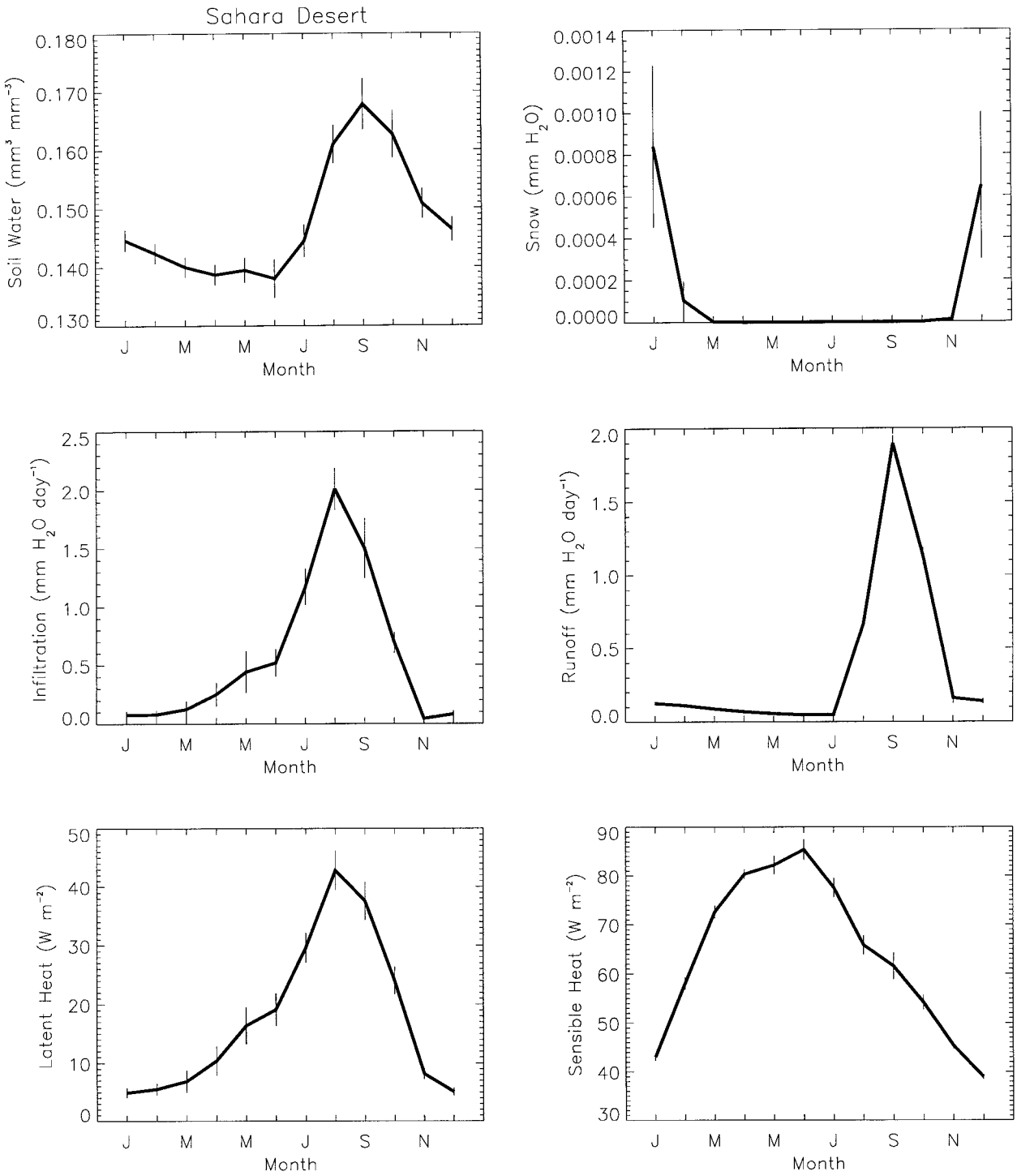

FIG. 14. Monthly features of the hydrologic cycle for the Sahara Desert and Arabian Peninsula (defined as all land points in an area bounded by 10°–30°N and 20°W–50°E). Soil water is the volume of water per unit volume of soil for the top 70 cm of soil. Runoff includes surface runoff and subsurface drainage. Vertical bars indicate the model's 95% confidence interval for the mean based on the 14-yr climatology.

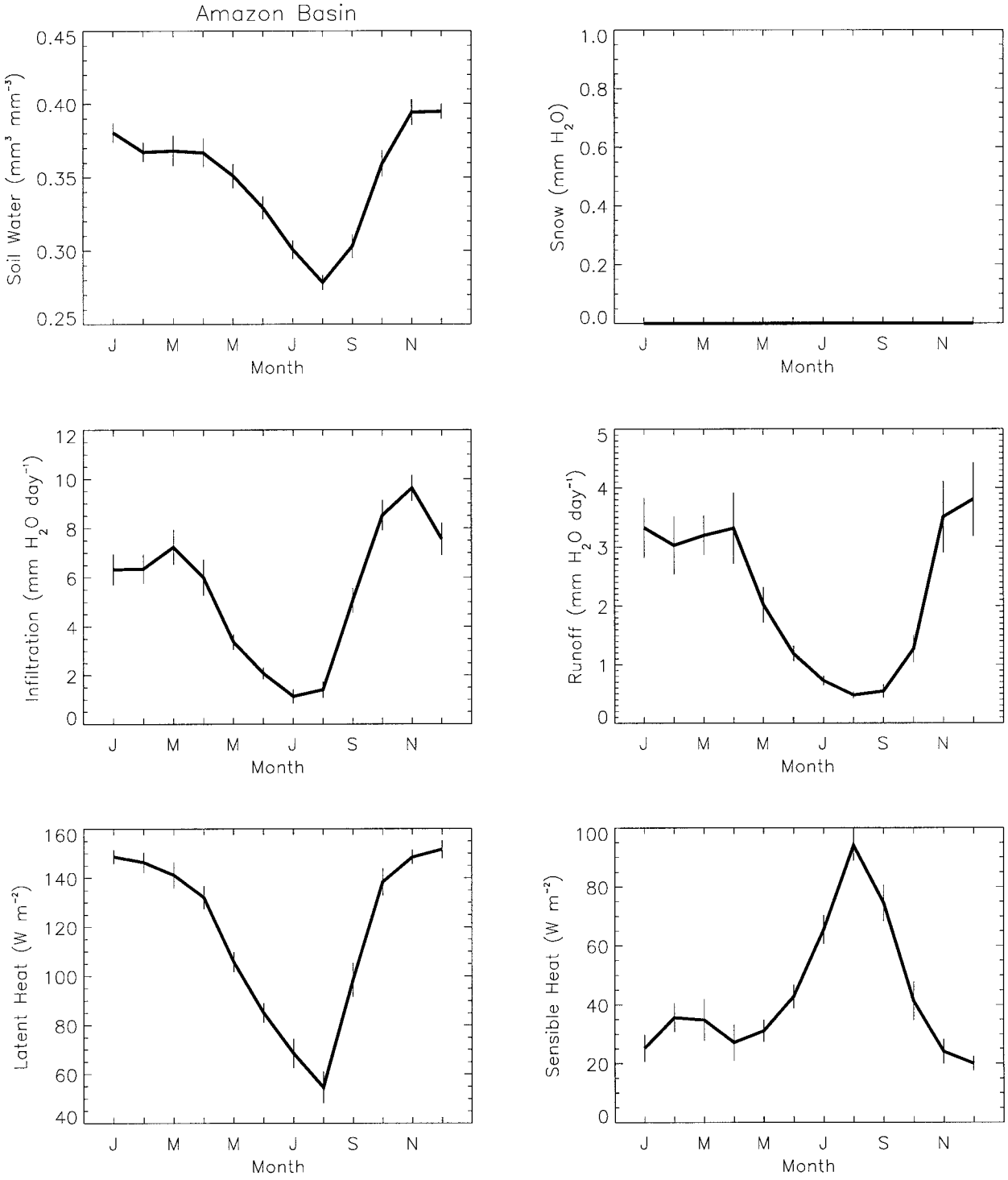

FIG. 15. As in Fig. 14 but for the Amazon Basin (10°S to the equator, 70°–50°W).

dra), Lieth's estimates are much higher than results from other models of terrestrial productivity. Overall, the net primary production simulated by LSM1.0 coupled to CCM3− is consistent with the best available estimates [see also Table 9 in Bonan (1996b)].

When coupled to CCM3, the model's net primary production is similar to that of the CCM3− simulation for all vegetation types except tropical broadleaf evergreen forest, mixed forest and crop, grassland, and crop (Table 3). In these vegetation types, net primary pro-

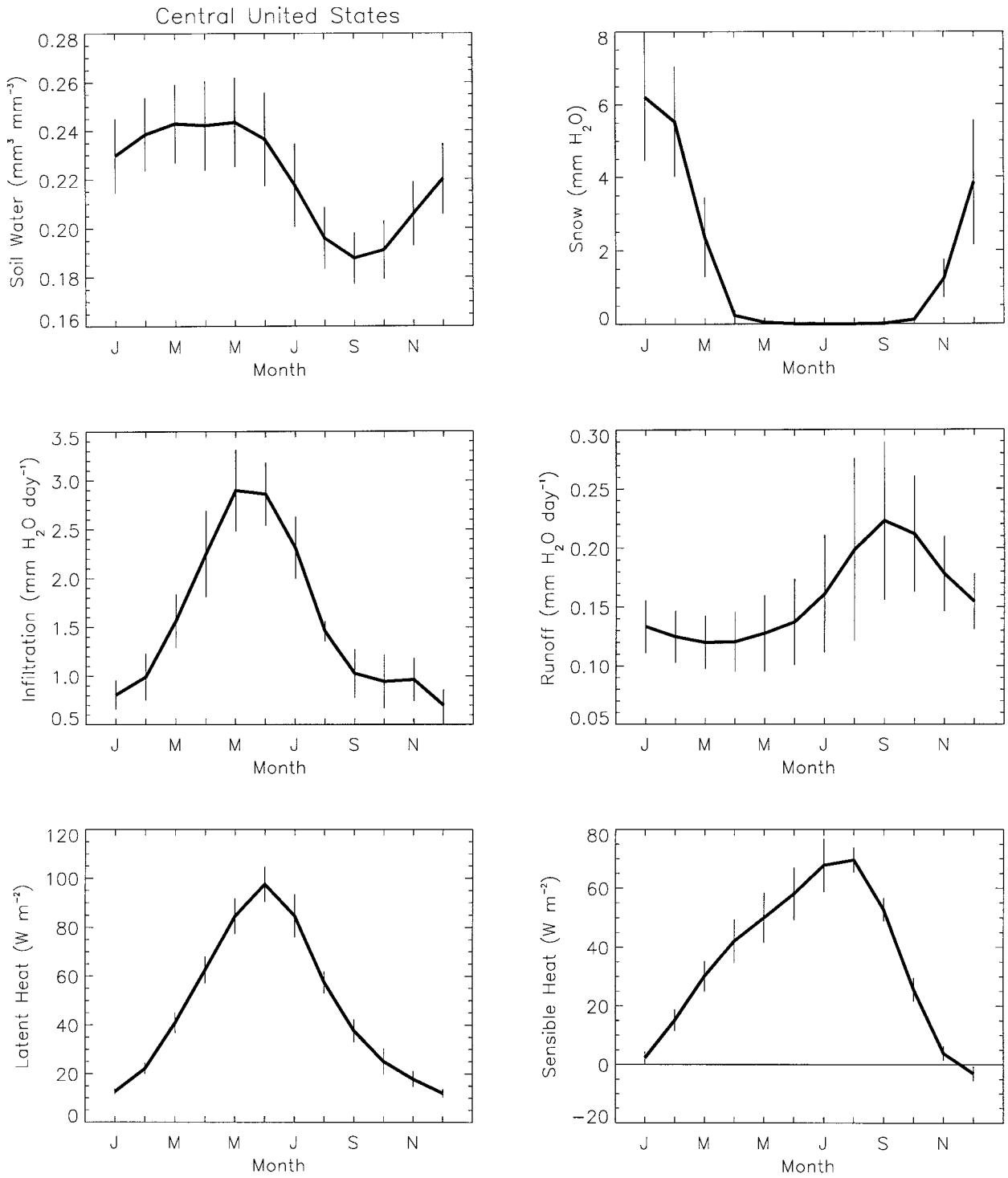

FIG. 16. As in Fig. 14 but for central United States (30°–50°N, 110°–90°W).

duction increases by 44%, 40%, 21%, and 31%, respectively. In each of these vegetation types, the biomass produced during photosynthesis increases dramatically compared to the CCM3− simulation (Table 4), possibly as a result of changes in soil water or atmospheric humidity—two important environmental constraints of stomatal resistance and CO_2 uptake. Leaf maintenance respiration also increases for these vegetation types (Table 5). However, for the tropical broadleaf evergreen forest and the forest crop, the propor-

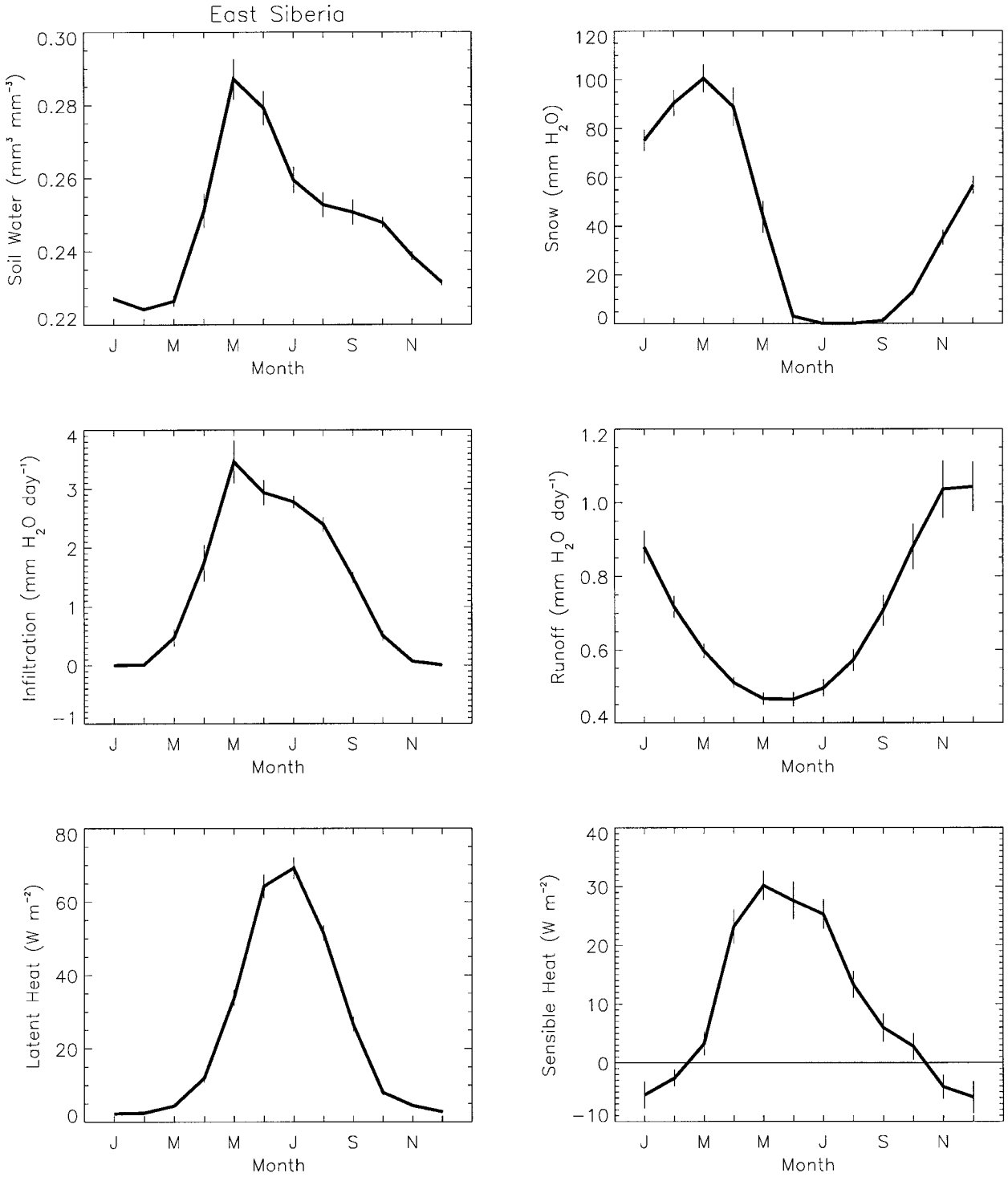

FIG. 17. As in Fig. 14 but for east Siberia (50°–70°N, 90°–140°E).

tional increase in leaf maintenance respiration is much less than the proportional increase in photosynthesis. Soil water is a common limiting factor for both photosynthesis and leaf maintenance respiration. Since leaf respiration does not respond in the same manner as photosynthesis, this suggests that soil water does not play a role in the increased photosynthesis. The increase most likely arises from changes in atmospheric humidity, which can severely limit photosynthesis. Changes in soil water appear to be more important in the grassland and

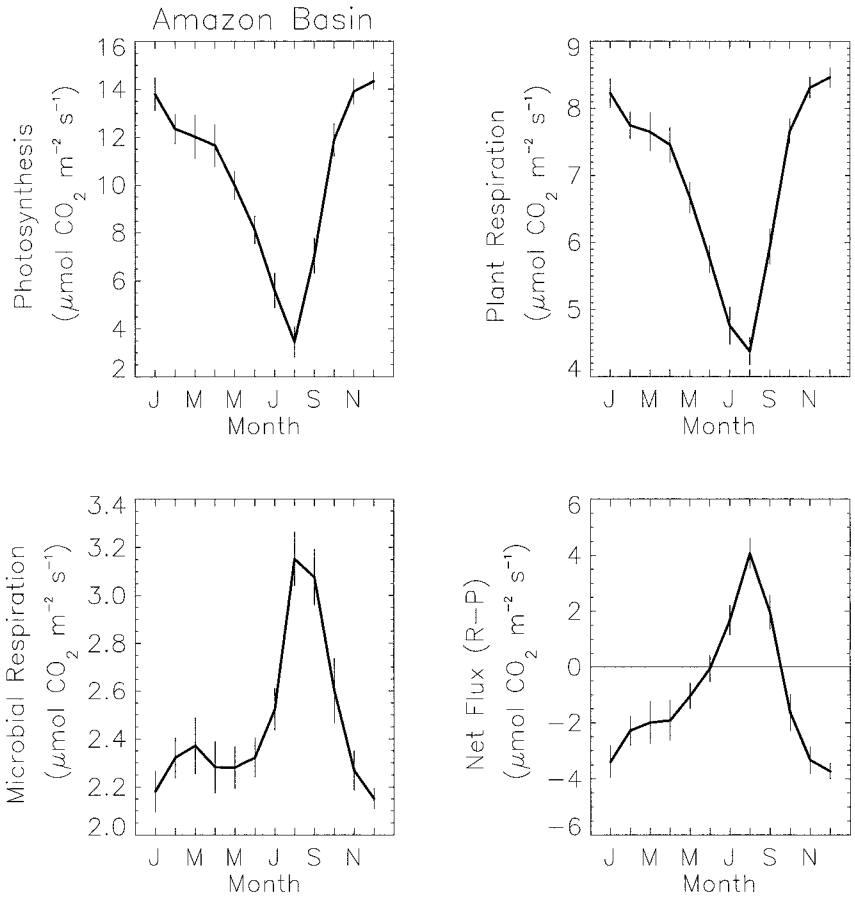

FIG. 18. Monthly CO_2 fluxes for the Amazon Basin region of South America. Plant respiration includes growth and maintenance respiration for foliage, stem, and root biomass. The net flux is the difference between CO_2 uptake during photosynthesis and CO_2 loss during plant and microbial respiration. A negative flux indicates net uptake. Vertical bars indicate the model's 95% confidence interval for the mean based on the 14-yr climatology. The Amazon Basin is defined as all land points in a box from 10°S to the equator and 70°–50°W.

crop vegetation, where the proportional increase in leaf respiration is similar to the proportional increase in photosynthesis. Stem and root maintenance respiration either decrease or change only slightly compared to the CCM3− simulation (Table 6). Since these fluxes depend only on temperature, increasing with warmer temperatures, this implies a general cooling of the surface.

The increase in net primary production for the tropical broadleaf evergreen forest, mixed forest and crop, grassland, and crop arise, then, because of large increases in photosynthesis, smaller increases in leaf maintenance respiration, and decreases in stem and root maintenance respiration. These problems can be alleviated by increasing the maintenance respiration costs. Stem and root respiration rates are poorly known and values for LSM1.0 were obtained by tuning stem and root respiration to give reasonable annual net primary production (Bonan 1995a, 1996a). Increasing the stem and root respiration rates per unit biomass [R_{s25} and R_{r25}, Table 17 in Bonan (1996a)] by a factor of 1.5 for the broadleaf evergreen tree, C_3 grass, and C_4 grass plant types would give net primary production similar to those in the CCM3− simulation. Crop maintenance respiration would have to be increased by a factor of 2.3.

The development of the atmospheric model has progressed beyond the standard CCM3 to include prognostic cloud water. A 14-yr simulation of this atmospheric model coupled to the land model (referred to as CCM3+ in Tables 3–7) shows a reduction in net primary production, compared to the CCM3 simulation, for all vegetation types (Table 3). For the needleleaf evergreen forest, tropical broadleaf evergreen forest, forest-crop, and tundra vegetation, this reduction exceeds 15% of the values for the CCM3 simulation. Photosynthesis and leaf maintenance respiration decrease for all vegetation types (Tables 4, 5). Both of these depend on soil water, suggesting a decrease in water availability. Stem and root maintenance respiration also decrease for all vegetation types. Since these respiration rates depend solely on temperature,

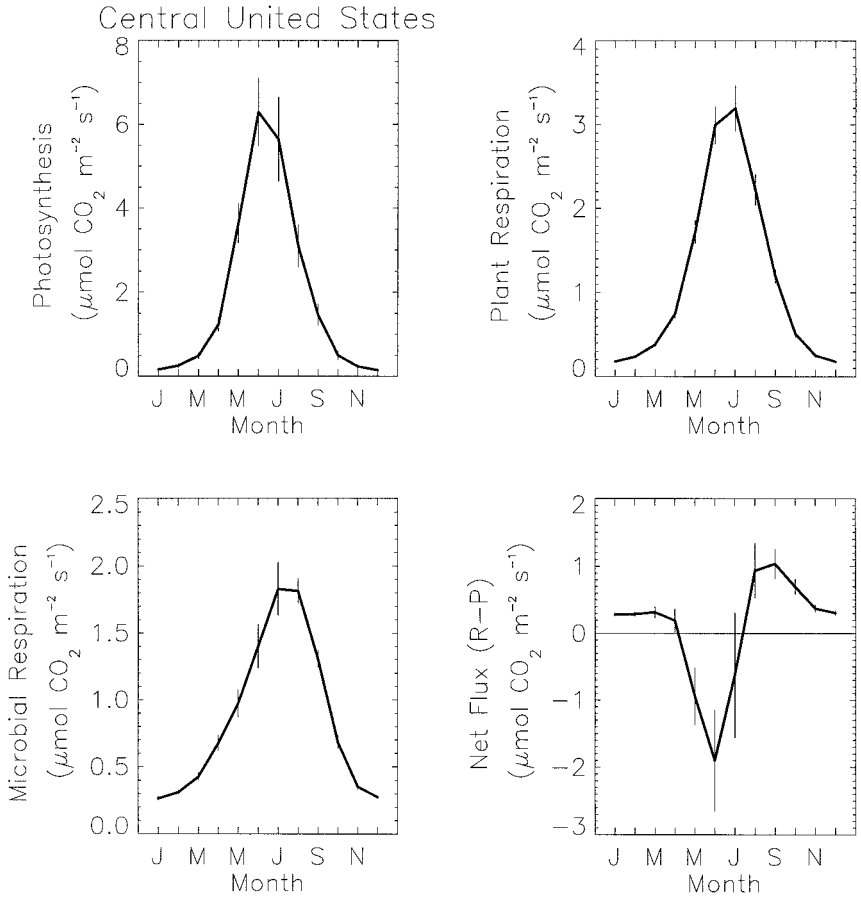

FIG. 19. As in Fig. 18 but for central United States (30°–50°N, 110°–90°W).

the lower respiration rates indicate colder surface temperatures.

Microbial respiration is much less sensitive to changes in the simulated climate. The differences in annual microbial respiration between the CCM3− and CCM3 simulations are less than ±10%. In the CCM3+ simulation, annual microbial respiration decreases for all vegetation types, which is expected from the overall surface cooling. However, these decreases are small.

Net CO_2 flux is the difference between CO_2 uptake during photosynthesis and CO_2 loss during plant and microbial respiration. When summed over all land points, the CCM3− simulation has the biosphere being a small (4×10^{12} g) annual source of CO_2 (Table 7). CO_2 loss from forest crop, shrubland, and semidesert vegetation are the primary causes of this efflux. In the CCM3 simulation, the biosphere is a large (29×10^{12} g) annual sink of CO_2. The primary cause of this is the greater plant production in tropical broadleaf evergreen forests, grasslands, and crops. In the CCM3+ simulation, the biosphere is still an annual CO_2 sink, but the magnitude has been reduced to less than one-half that of the CCM3 simulation. This largely reflects decreased plant production in all vegetation types. In both the CCM3 and CCM3+ simulations, tropical forests account for the vast majority of the difference in the global flux.

4. Discussion and summary

The CCM3 coupled to LSM1.0 simulates many of the observed geographic and seasonal patterns of surface air temperature and precipitation. In general, the transition seasons (spring, autumn) are better simulated than winter and summer. Some important biases are the following: desert and arid regions are too cold in winter and summer although precipitation is well simulated; winter temperatures are several degrees too warm in North America extending from central Canada northwest to Alaska and in Asia extending from the Caspian Sea northeast to Siberia; summer temperatures are 2.5°–5°C too cold in much of Alaska, northwest Canada, northern Europe, Russia, and western Asia; precipitation is overestimated in highlatitudes of the Northern Hemisphere throughout the year. The winter warm biases are present in the CCM even without the land model, although the coupling with the land model accentuates the biases (Bonan 1996b) and the likely solution lies in the atmospheric physics. The land model cools much of the Northern Hemisphere in summer, causing the sum-

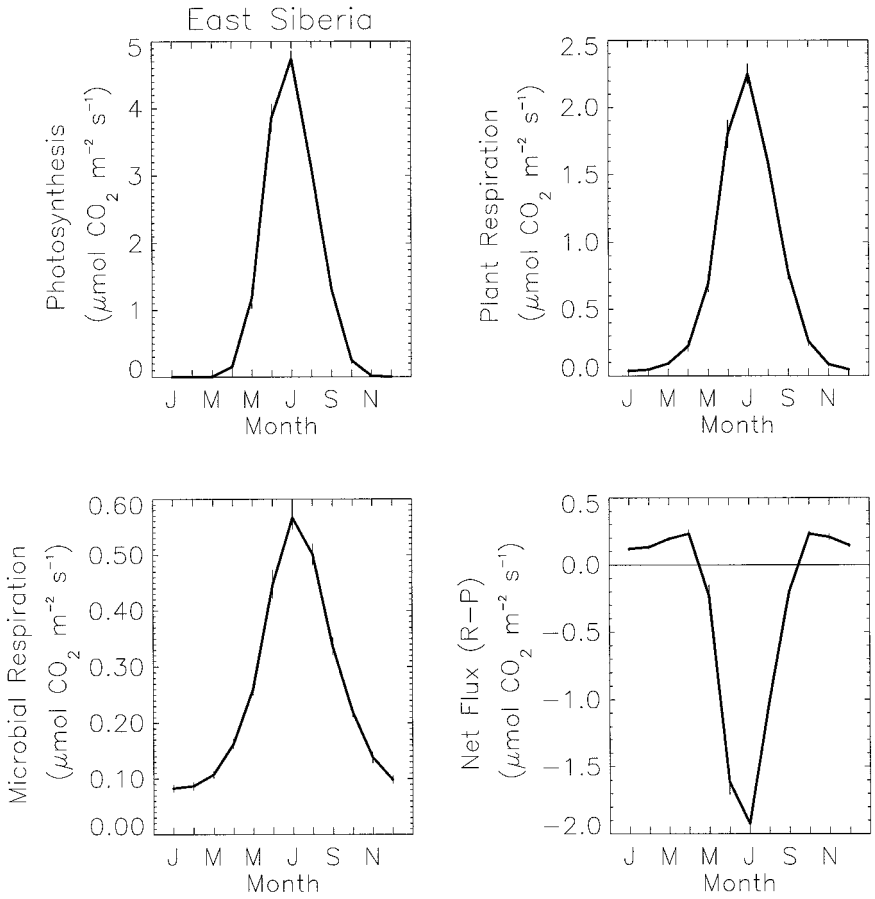

FIG. 20. As in Fig. 18 but for east Siberia (50°–70°N, 90°–140°E).

TABLE 3. Annual net primary production (grams of biomass m^{-2} yr^{-1}) averaged by vegetation type for Lieth's estimates and three simulations in which the land model was coupled to different versions of the CCM3: CCM3−, average for a 5-yr simulation. CCM3, average for a 14-yr simulation. [* indicates net primary production (NPP) differs from CCM3− by more than 15%.] CCM3+, average for a 14-yr simulation (* indicates NPP differs from CCM3 by more than 15%). Net primary production is equal to photosynthesis (Table 4) minus leaf maintenance respiration (Table 5) minus stem and root maintenance respiration (Table 6).

Vegetation type	Cells	Area (10^6 km^2)	Net primary production (g m^{-2} yr^{-1})			
			Lieth	CCM3−	CCM3	CCM3+
No vegetation						
Glacier	841	14.8	—	0	0	0
Desert	80	5.2	—	0	0	0
Forest						
Needleleaf evergreen tree	146	7.9	705	516	553	434*
Needleleaf deciduous tree	54	2.8	373	352	341	314
Broadleaf deciduous tree	25	2.0	1567	1129	1040	970
Mixed needle- and broadleaf tree	56	3.3	811	893	1008	886
Tropical broadleaf evergreen tree	159	15.2	2251	2311	3322*	2775*
Interrupted woods						
Savanna	138	13.0	1592	1214	1305	1179
Evergreen forest tundra	66	3.2	470	382	375	322
Deciduous forest tundra	88	3.6	285	315	278	241
Mixed forest and crop	128	9.1	—	837	1170*	989*
Nonwoods						
Grassland	315	25.2	895	698	846*	770
Tundra	225	9.4	425	257	246	204*
Shrubland	91	8.0	—	219	205	201
Semidesert	177	14.6	—	11	9	8
Crop	160	11.8	—	1038	1357*	1258

TABLE 4. Annual photosynthesis (grams of biomass m^{-2} yr^{-1}) averaged by vegetation type for the CCM3−, CCM3, and CCM3+ simulations. Growth respiration (25% of photosynthesis) has been subtracted from the total. CO_2 fluxes are converted to biomass assuming 28.5 grams biomass are produced per mole of CO_2 exchanged. The * indicates vegetation types with large differences in net primary production (Table 3).

Vegetation type	Cells	Area (10^6 km^2)	Photosynthesis (g m^{-2} yr^{-1})		
			CCM3−	CCM3	CCM3+
No vegetation					
Glacier	841	14.8	0	0	0
Desert	80	5.2	0	0	0
Forest					
Needleleaf evergreen tree	146	7.9	1675	1623	1456*
Needleleaf deciduous tree	54	2.8	479	456	421
Broadleaf deciduous tree	25	2.0	1472	1344	1264
Mixed needle- and broadleaf tree	56	3.3	1657	1737	1581
Tropical broadleaf evergreen tree	159	15.2	5757	6812*	6141*
Interrupted woods					
Savanna	138	13.0	2726	2781	2617
Evergreen forest tundra	66	3.2	700	665	597
Deciduous forest tundra	88	3.6	410	361	316
Mixed forest and crop	128	9.1	2197	2467*	2249*
Nonwoods					
Grassland	315	25.2	1177	1343*	1251
Tundra	225	9.4	373	355	303*
Shrubland	91	8.0	283	262	257
Semidesert	177	14.6	13	11	10
Crop	160	11.8	1247	1610*	1499

mer cold bias (Bonan 1996b). This cold bias appears to be caused by wet soils in which latent heat is a high portion of net radiation. Comparisons of observed and simulated surface fluxes for several boreal forest sites in Canada (Bonan et al. 1997) and several tundra sites in Alaska (unpublished) should give further insights to the cause of this cold bias.

The land model reproduces expected seasonal and geographic patterns of soil water. In temperate and cold climates, soil water is depleted beginning in late spring and continuing through summer, with recharge in fall, winter, and early spring. Spring snowmelt is an important source of water to recharge the dry soils. In the Tropics, soils recharge during the rainy season. In general, the land model simulates decreased latent heat flux, increased sensible heat flux, and decreased CO_2 uptake during periods of soil water depletion.

Annual precipitation and runoff are well simulated for some river basins and poorly simulated for others. In general, precipitation is better simulated than runoff.

TABLE 5. As in Table 4 but for annual leaf maintenance respiration.

Vegetation type	Cells	Area (10^6 km^2)	Leaf respiration (g m^{-2} yr^{-1})		
			CCM3−	CCM3	CCM3+
No vegetation					
Glacier	841	14.8	0	0	0
Desert	80	5.2	0	0	0
Forest					
Needleleaf evergreen tree	146	7.9	247	221	203*
Needleleaf deciduous tree	54	2.8	57	51	48
Broadleaf deciduous tree	25	2.0	259	218	209
Mixed needle- and broadleaf tree	56	3.3	248	242	229
Tropical broadleaf evergreen tree	159	15.2	1602	1691*	1591*
Interrupted woods					
Savanna	138	13.0	513	481	458
Evergreen forest tundra	66	3.2	86	75	69
Deciduous forest tundra	88	3.6	41	36	31
Mixed forest and crop	128	9.1	409	413*	388*
Nonwoods					
Grassland	315	25.2	192	214*	202
Tundra	225	9.4	37	34	30*
Shrubland	91	8.0	63	57	56
Semidesert	177	14.6	3	2	2
Crop	160	11.8	209	253*	241

TABLE 6. As in Table 4 but for annual stem and root maintenance respiration.

Vegetation type	Cells	Area (10^6 km^2)	Stem + root respiration (g m^{-2} yr^{-1})		
			CCM3−	CCM3	CCM3+
No vegetation					
Glacier	841	14.8	0	0	0
Desert	80	5.2	0	0	0
Forest					
Needleleaf evergreen tree	146	7.9	912	849	819*
Needleleaf deciduous tree	54	2.8	70	64	60
Broadleaf deciduous tree	25	2.0	83	87	84
Mixed needle- and broadleaf tree	56	3.3	517	488	466
Tropical broadleaf evergreen tree	159	15.2	1845	1800*	1776*
Interrupted woods					
Savanna	138	13.0	999	994	980
Evergreen forest tundra	66	3.2	233	215	206
Deciduous forest tundra	88	3.6	52	47	43
Mixed forest and crop	128	9.1	950	883*	872*
Nonwoods					
Grassland	315	25.2	288	282*	278
Tundra	225	9.4	79	75	70*
Shrubland	91	8.0	0	0	0
Semidesert	177	14.6	0	0	0
Crop	160	11.8	0	0*	0

The problem, as noted in Bonan (1996c), is that precipitation can either infiltrate into the soil, in which case runoff may be underestimated but the wet soils sustain a high latent heat flux that cools the surface, or it can run off, in which case the dry soils create a warm surface. This is especially important in the Mississippi River Basin, where the model is already slightly warm in summer but where annual runoff is only one-third the annual observed river flow.

The inclusion of net land–atmosphere CO_2 exchange is an important component of the land model, allowing it to be used for studies of the global carbon cycle in a manner similar to the SiB2 model (Denning et al. 1995, 1996a,b). The model simulates annual net primary production that is consistent with other estimates of annual production. The model also simulates a clearly defined growing season. In temperature grasslands, forests, and crops, in boreal forests, and in arctic tundra, peak rates of photosynthesis, plant respiration, microbial respiration, and net CO_2 uptake occur during the summer.

TABLE 7. Annual net CO_2 flux (respiration–photosynthesis) averaged by vegetation type for three simulations with different versions of the CCM3: CCM3−, average for a 5-yr simulation; CCM3, average for a 14-yr simulation (* indicates the net flux differs from CCM3− by more than 50%); and CCM3+, average for a 14-yr simulation (* indicates the net flux differs from CCM3 by more than 50%).

Vegetation type	Cells	Area (10^6 km^2)	Net flux (10^{12} g CO_2 yr^{-1})		
			CCM3−	CCM3	CCM3+
No vegetation					
Glacier	841	14.8	0.00	0	0
Desert	80	5.2	0.00	0	0
Forest					
Needleleaf evergreen tree	146	7.9	−0.79	−1.35*	−0.40*
Needleleaf deciduous tree	54	2.8	−0.39	−0.40	−0.35
Broadleaf deciduous tree	25	2.0	−0.09	0.28*	0.36
Mixed needle- and broadleaf tree	56	3.3	−1.54	−2.03	−1.65
Tropical broadleaf evergreen tree	159	15.2	−5.47	−23.57*	−14.60
Interrupted woods					
Savanna	138	13.0	0.44	−0.62*	1.04*
Evergreen forest tundra	66	3.2	−0.91	−0.92	−0.74
Deciduous forest tundra	88	3.6	−0.82	−0.71	−0.59
Mixed forest and crop	128	9.1	4.67	0.48*	2.22*
Nonwoods					
Grassland	315	25.2	−0.07	−3.88*	−2.10
Tundra	225	9.4	−2.03	−1.95	−1.54
Shrubland	91	8.0	9.32	9.37	9.35
Semidesert	177	14.6	2.08	1.93	1.90
Crop	160	11.8	−0.28	−5.93*	−4.81
Total	2749	148.8	4.11	−29.31*	−11.92*

These areas are small sources of CO_2 during the rest of the year. In the Tropics, maximum rates of photosynthesis, plant respiration, and net CO_2 uptake occur during the rainy season. Comparisons with annual and monthly satellite-derived vegetation indices (e.g., NDVI) would help clarify the geographic and seasonal patterns simulated by the model.

Simulations in which the land CO_2 fluxes are transported with the atmospheric model to simulate atmospheric CO_2 concentrations show the model is a useful tool to better understand the biosphere's role in the global carbon cycle (Craig et al. 1998). However, the large differences in simulated CO_2 fluxes arising from improvements in the atmospheric model (Tables 3 and 7) demonstrate the extreme sensitivity of land–atmosphere CO_2 exchange to the simulated climate. Moreover, the leaf, stem, and root carbon pools in the model, as well as the geographic distribution of vegetation types, are time invariant. This may introduce situations where the simulated fluxes are inconsistent with the prescribed vegetation. The solution to this problem requires adding new ecological submodels to the land surface model. Biogeochemical processes, in which carbon is allocated within the vegetation, falls to the ground as litter, and decomposes, are needed to simulate seasonal to annual changes in carbon pools. Long-term successional processes such as migration, reproduction, mortality, and differential life history characteristics allow the type of vegetation to change over decades, centuries, and millenia. Much more research is needed to understand how to best parameterize these ecological processes.

REFERENCES

Baumgartner, A., and E. Reichel, 1975: *The World Water Balance: Mean Annual Global, Continental and Maritime Precipitation, Evaporation, and Run-Off.* Elsevier, 179 pp.

Bonan, G. B., 1995a: Land–atmosphere CO_2 exchange simulated by a land surface process model coupled to an atmospheric general circulation model. *J. Geophys. Res.,* **100** (D), 2817–2831.

——, 1995b: Sensitivity of a GCM simulation to inclusion of inland water surfaces. *J. Climate,* **8,** 2691–2704.

——, 1996a: A land surface model (LSM version 1.0) for ecological, hydrological, and atmospheric studies: Technical description and user's guide. NCAR Tech. Note NCAR/TN-417+STR, 150 pp. [Available from NCAR, P.O. Box 3000, Boulder, CO 80307.]

——, 1996b: The NCAR Land Surface Model (LSM version 1.0) coupled to the NCAR Community Climate Model. NCAR Tech. Note NCAR/TN-429+STR, 171 pp. [Available from NCAR, P.O. Box 3000, Boulder, CO 80307.]

——, 1996c: Sensitivity of a GCM simulation to subgrid infiltration and surface runoff. *Climate Dyn.,* **12,** 279–285.

——, 1997: Effects of land use on the climate of the United States. *Climate Change,* **37**, 449–486.

——, K. J. Davis, D. Baldocchi, D. Fitzjarrald, and H. Neumann, 1997: Comparison of the NCAR LSM1 land surface model with BOREAS aspen and jack pine tower fluxes. *J. Geophys. Res.,* **102**, 29 065–29 075.

Coe, M. T., and G. B. Bonan, 1997: Feedbacks between climate and surface water in northern Africa during the middle Holocene. *J. Geophys. Res.,* **102,** 11 087–11 101.

Craig, S. G., K. J. Holmén, G. B. Bonan, and P. J. Rasch, 1998: Atmospheric CO_2 simulated by the NCAR Community Climate Model. Part I: Mean fields and seasonal cycles. *J. Geophys. Res.,* in press.

Denning, A. S., I. Y. Fung, and D. A. Randall, 1995: Latitudinal gradient of atmospheric CO_2 due to seasonal exchange with land biota. *Nature,* **376,** 240–243.

——, G. J. Collatz, C. Zhang, D. A. Randall, J. A. Berry, P. J. Sellers, G. D. Colello, and D. A. Dazlich, 1996a: Simulations of terrestrial carbon metabolism and atmospheric CO_2 in a general circulation model. Part 1: Surface carbon fluxes. *Tellus,* **48B,** 521–542.

——, D. A. Randall, G. J. Collatz, and P. J. Sellers, 1996b: Simulations of terrestrial carbon metabolism and atmospheric CO_2 in a general circulation model. Part 2: Simulated CO_2 concentrations. *Tellus,* **48B,** 543–567.

Kutzbach, J., G. Bonan, J. Foley, and S. P. Harrison, 1996: Vegetation and soil feedbacks on the response of the African monsoon to orbital forcing in the early to middle Holocene. *Nature,* **384,** 623–626.

Legates, D. R., and C. J. Willmott, 1990a: Mean seasonal and spatial variability in global surface air temperature. *Theor. Appl. Climatol.,* **41,** 11–21.

——, and ——, 1990b: Mean seasonal and spatial variability in gauge-corrected, global precipitation. *Int. J. Climatol.,* **10,** 111–127.

Mintz, Y., and G. K. Walker, 1993: Global fields of soil moisture and land surface evapo-transpiration derived from observed precipitation and surface air temperature. *J. Appl. Meteor.,* **32,** 1305–1334.